Journal of Solid State Chemistry 181 (2008) 2507–2515

Contents lists available at ScienceDirect

Journal of Solid State Chemistry

journal homepage: www.elsevier.com/locate/jssc

Anchored thiol smectite clay—kinetic and thermodynamic studies of divalent copper and cobalt adsorption

Denis Lima Guerra *, Claudio Airoldi

Instituto de Química, Universidade Estadual de Campinas, Caixa Postal 6154, 13084-971 Campinas, São Paulo, Brasil

ARTICLE INFO

Article history:
Received 23 February 2008
Received in revised form
5 June 2008
Accepted 14 June 2008
Available online 19 June 2008

Keywords:
Smectite
Adsorption isotherms
Kinetic
Thermodynamic

ABSTRACT

A natural smectite clay sample from Serra de Maicuru, Pará State, Brazil, had aluminum and zirconium polyoxycations inserted within the interlayer space. The precursor and pillarized smectites were organofunctionalized with the silyating agent 3-mercaptopropyltrimethoxysilane. The basal spacing of 1.47 nm for natural clay increased to 2.58 and 2.63 nm, for pillared aluminum, $S_{Al/SH}$, and zirconium, $S_{Zr/SH}$, and increases in the surface area from 44 to 583 and 585 $m^2 g^{-1}$, respectively. These chemically immobilized clay samples adsorb divalent copper and cobalt cations from aqueous solutions of pH 5.0 at 298 ± 1 K. The Langmuir, Redlich–Peterson and Toth adsorption isotherm models have been applied to fit the experimental data with a nonlinear approach. From the cation/basic center interactions for each smectite at the solid–liquid interface, by using van't Hoff methodology, the equilibrium constant and exothermic thermal effects were calculated. By considering the net interactive number of moles for each cation and the equilibrium constant, the enthalpy, $\Delta_{int}H^0$ (-9.2 ± 0.2 to -10.2 ± 0.2 kJ mol^{-1}) and negative Gibbs free energy, $\Delta_{int}G^0$ (-23.9 ± 0.1 to -28.7 ± 0.1 kJ mol^{-1}) were calculated. These values enabled the positive entropy, $\Delta_{int}S^0$ (51.3 ± 0.3 to 55.0 ± 0.3 JK^{-1} mol^{-1}) determination. The cation-sulfur interactive process is spontaneous in nature, reflecting the favorable enthalpic and entropic results. The kinetics of adsorption demonstrated that the fit is in agreement with a second-order model reaction with rate constant k_2, varying from 4.8×10^{-2} to 15.0×10^{-2} and 3.9×10^{-2} to 12.2×10^{-2} $mmol^{-1}$ min^{-1} for copper and cobalt, respectively.

1. Introduction

Smectite is generated from soils and sedimentary deposits through weathering, diagenesis and hydrothermal effects. This process involves degradation and transformation of precursor phyllosilicates, including precipitation from solution. Thus, clays derived from various abundant minerals in soils, influenced by conditions that contain basic igneous rocks and also soil clay fractions from arid climates, originating from granitic pediment [1–8]. Such kinds of smectite samples can be found naturally in the Amazon region; however, this smectite occurrence is rare due to the fact that the Amazon climate is normally warm-humid, causing acidic lixiviation in soils, conditions that are unfavorable to smectite formation [9].

Taking into account pristine smectite chemical composition with original acidic or basic active functions, useful for surface chemical modification, through inclusion of some other active groups, then, the possibility of application is significantly increased, including those related to cation removal from waters, simulating also wastewater effluents [9]. For this purpose, copper and cobalt were chosen for the present investigation due to the fact that these metals can be discharged to the environment, arising, for example, from paint production, pharmaceutical and industrial chemical processes and may cause damage to soil, aquatic media, fauna and flora [6]. To eliminate these undesirable poisons from an ecosystem, several methods have been proposed, such as electrodeposition, solvent extraction, membrane and separation, adsorption on activated or/and chemically modified clays [7–10].

The aim of the present investigation is focused on the retention capacities and thermal effects of a smectite from the Amazon region, as received and when chemically modified, for adsorbing divalent copper and cobalt. The natural matrix was pillared with aluminum and zirconium polyoxycations and for the first time organofunctionalized with the silyating agent 3-mercaptopropyltrimethoxysilane. The adsorption process was fitted to Langmuir, Redlich–Peterson and Toth models for nonlinear regression methods. The energetic effect caused by the divalent cation/sulfur basic center on smectite interactions at the solid/liquid interface was determined through the van't Hoff procedure and a kinetic

* Corresponding author.
E-mail address: dlguerra@iqm.unicamp.br (D.L. Guerra).

0022-4596/$ - see front matter © 2008 Published by Elsevier Inc.
doi:10.1016/j.jssc.2008.06.028

study was performed by adjusting to pseudo-second-order Lagergren models.

2. Experimental

2.1. Raw material

The sampled (*S*) clay from the Serra de Maicuru area, State of Pará, northern Brazil with particle size less than 2 μm, was separated by sedimentation. The cation-exchange capacity was evaluated through intercalation with 2.0 mol dm^{-3} ammonium acetate at pH 8.0 [9], to give an exchange of 1.15 mmol g^{-1}.

2.2. Sample preparation

The natural clay sample was ground and sieved through a USS (200 mesh) 0.074 mm, sieve, dried in an oven at 333 K to reach humidity between 12% and 15%, as followed by the thermogravimetric technique. A preliminary X-ray powder diffractometry analysis was used to confirm the presence of the smectite clay fraction through conventional procedures: air-dried, ethylene glycol solvated and heated at 573 and 773 K [9].

2.3. Chemical modification

An OH/Al = 2.0 molar ratio solution was obtained by slow dropwise addition of 0.20 mol dm^{-3} sodium hydroxide to a 0.20 mol dm^{-3} aqueous $AlCl_3 \cdots 6H_2O$ solution, under vigorous stirring at 333 K [2].

The zirconium solution was prepared by adding appropriate volumes of 0.10 mol dm^{-3} aqueous $ZrOCl_2 \cdots 8H_2O$ solution directly to the smectite suspension at room temperature with vigorous stirring [8].

Two portions of 5.0 g of natural smectite *S* were suspended in 100.0 cm^3 of the pillaring solutions at room temperature under vigorous stirring for 25 h. The resulting suspensions were centrifuged at 4000 rpm for 60 min. The liquid was decanted to prevent the finer particles from re-entering suspensions and the washed solids with water were dried at 323 K for 17 h, to result in samples named S_{Al} and S_{Zr}.

A mass of 5.0 g of each pillared smectite sample was suspended with 5.0 cm^3 of the silylating agent 3-mercaptopropyltrimethoxysilane in xylene under reflux at inert nitrogen atmosphere and with mechanical stirring for 3 h. The solution was filtered through sintered glass, washed several times with water and the solid was dried under vacuum for 12 h, to give the respective $S_{Al/SH}$ and $S_{Zr/SH}$ matrices.

2.4. Adsorption

Samples of about 50 mg of the natural or chemically modified smectites were suspended in 20.0 cm^3 of aqueous metallic solutions, varying in concentration from 7.0×10^{-3} to 7.0×10^{-4} mol dm^{-3} at 298 ± 1 K, to carry out the adsorption process. Firstly, the effect of pH on adsorption for natural and anchored samples was evaluated by varying through the 1.0–5.0 range, by the addition of 0.10 mol dm^{-3} of nitric acid or 0.10 mol dm^{-3} sodium hydroxide.

The isotherms of concentration versus time were obtained through a batch method [10–12]. The number of moles adsorbed per gram (N_f) is calculated by the difference between the initial (N_i) and the remaining number of moles of metal in the supernatant (N_s) divided by the mass (m) of the compound used, Eq. (1).

$$N_f = \frac{(N_i - N_S)}{m} \tag{1}$$

The same procedure was used to obtain the isotherms of concentration versus time and the maxima adsorption capacity was identically calculated. The number of moles of cation adsorbed (N_f) increased with concentration in the supernatant (C_s) as a function of pH and time (t), until the plateau related to total saturation of the acidic centers in the layered structure was obtained [10–12].

The most commonly used isotherms are those related to Langmuir, which was originally derived for gas adsorption on planar surfaces such as glass, mica and platinum. The process was successfully extended to heavy metal ion adsorptions on porous surfaces. For this adsorption model, a quantity adsorbed is related to the equilibrium solution concentration of the adsorbate, after adjusting to K_L and b parameters. The plateau of the isotherm enables K_L determination that reflected the affinity of the adsorbate on the surface. The b value is the upper limit and represents the maximum adsorption, determined by the number of reactive surface sites [10–12], as represented by

$$N_f = \frac{K_L b C_S}{1 + b C_S} \tag{2}$$

Then, C_s/N_f and the so-called distribution coefficient K_L can be plotted against the concentration of the supernatant. If the Langmuir equation can be adjusted to the system, the measured data should fall on a straight line, whose slope gives K_L and the intercept b values, derived from $1/K_L b$ and $1/b$. These being the angular and linear coefficients [10–18], as represented by

$$\left[\frac{C_S}{N_f}\right] = \left[\frac{1}{(K_L b)}\right] + \left[\frac{C_S}{b}\right] \tag{3}$$

Another fitting for the adsorption process is established by the Redlich–Peterson (Eq. (4)) and Toth (Eq. (5)) equations:

$$N_f = K_{RP} b C_S / (1 + K_{RP} C_S^{\beta}) \tag{4}$$

$$N_f = K_T b C_S / (1 + K_T C_S^{\beta})^{1/\beta} \tag{5}$$

where K_{RP} and K_T are constants related to adsorption capacity and β is an affinity constant of the adsorbent. Although this equation was previously employed empirically, it can be derived with the assumption of a continuous variation in thermal effect during the adsorption process. There is no assurance that the derivations of the Redlich–Peterson and Toth equations are unique; consequently, if the collected data can fit to the equations, it is only likely, but not proven, that the surface is heterogeneous. The Redlich–Peterson and Toth models unfortunately predict both infinite adsorption at infinite concentration and a corresponding thermal effect related to the adsorption at zero coverage [13].

Nonlinear regression was compared to obtain the optimum kinetic sorption and isothermic parameters. A trial and error procedure was employed for nonlinear methods using the solver add-in functions of Microsoft Excel software. In the trial and error procedure, isotherm and kinetic parameters were determined by maximizing the coefficient of determination values [13]. The least-squares method was used to analyze the linear forms of the kinetic and isotherm models.

Coefficient of determination values (r^2) were used in order to find the fitting degrees of isotherm adsorption and kinetic models by considering the experimental data [13], as defined by

$$r^2 = \frac{\Sigma(N_{fCAL} - N_{fEXP})^2}{\Sigma(N_{fCAL} - N_{fEXP})^2 + (N_{fCAL} - N_{fEXP})^2} \tag{6}$$

where N_{fEXP} (mmol g^{-1}) is the experimental amount of divalent cations exchanged by the natural and the modified smectite and N_{fCAL} is the amount of cations obtained by kinetic and isotherm models [13].

2.5. Analytical procedures

The natural *S* clay sample was analyzed by Inductively Coupled Plasma-Optical Emission Spectrometry, using an ARL 34000 instrument.

X-ray powder diffraction patterns were recorded with a Philips PW 1050 diffractometer using Cu*K*α (0.154 nm) radiation in the 2–65° (2θ) region at a speed of 2° min^{-1} and a step of 0.050°.

Brunauer–Emmett–Teller (BET) surface areas and porosity measurements of the natural and modified samples were determined using a Quantachome/Nova Surface Area-Pore Volume Analyzer, Model 1200/5.01. The mesopore size distribution was obtained by applying the Barret–Joyner–Halenda (BJH) method to the adsorption branch of the isotherm.

For infrared spectroscopy, the samples were oven-dried at 393 K to remove any adsorbed water. Each sample of about 1.3 mg was finely ground for 1 min, combined with 100 mg of oven-dried spectroscopic-grade KBr and pressed with 7.0 tonnes into a disc under vacuum. The spectra of each sample was recorded in triplicate between 1250 and 4000 cm^{-1} by accumulating 64 scans at 4 cm^{-1} resolution, using a Perkin–Elmer 1760X Fourier transform infrared spectrometer.

The nuclear magnetic resonance spectra of natural and organofunctionalized smectite samples were obtained on an AC 300/P Bruker spectrometer at 298 ± 1 K at 59.6 MHz for silicon. A pulse repetition time of 3 s and contact time of 3 ms were used for ^{29}Si CPMAS experiments.

3. Results and discussion

3.1. Elemental analysis

The elemental analysis of the natural sample *S* gave results consistent with smectite, with aluminum and iron being the major elemental quantities contained in the well-organized structure, by presenting the chemical composition 55.56%; 13.42%; 9.78%; 1.76%; 1.30%; 0.97% and 0.98% of SiO_2, Al_2O_3, Fe_2O_3, MgO, Na_2O, CaO and K_2O, respectively, and 15.23% in mass was lost in the ignition process. Thus, the composition of this natural smectite, calculated from the chemical analysis, gives the formula:

$$(Na_{0.18}K_{0.09})(Al_{1.13}Mg_{0.19}Fe_{0.79}Ca_{0.07})(Si_{4.00}O_{10})(OH)_2 \quad (7)$$

3.2. X-ray and textural analysis

The natural smectite interlayer distance changed after chemical modification as shown in Fig. 1. An increase in d_{001} value was observed in the diffraction patterns, by changing from 1.48 to 2.58 and 2.63 nm for pillared $S_{Al//SH}$ and $S_{Zr/SH}$, respectively, as listed in Table 1. As expected, the silylating agent can covalently bond inside the free cavity formed by smectite layers and also by the introduced pillars, through the reaction of the available hydroxyl groups of the internal inorganic surfaces [14]. Based on the inorganic tetrahedral–octahedral–tetrahedral smectite arrangement with a layer thickness of 0.89 nm [19], the immobilized pendant chains can be accommodated along 0.59, 1.69 and 1.74 nm, into the free cavity space. However, another favorable possibility can occur when the pendant chains lie parallel to inorganic layers, as successive pillars are removed.

The gaseous nitrogen adsorption values for natural and modified smectite samples are also listed in Table 1. The specific surface areas were calculated by the BET method, in order to compare these three matrices. Thus, the BET surface areas demonstrated that pillarization and organofunctionalization caused micropore formation in the solid particles, resulting in a higher surface areas, from natural smectite *S* with 44 $m^2 g^{-1}$ to 583 and 585 $m^2 g^{-1}$ related to $S_{Al/SH}$ and $S_{Zr/SH}$, respectively. The pore size distribution in the mesopore region was obtained by comparing natural and modified samples, applying the BJH method to the nitrogen isotherms at 77 K. The samples contain mostly mesopores, where the natural smectite *S* shows a pore volume of 1.6 $cm^3 g^{-1}$, which increases to 2.7 and 3.7 $cm^3 g^{-1}$ for $S_{Al/SH}$ and $S_{Zr/SH}$, respectively. The pore diameter changes in the same direction, varying from 0.13 nm for the natural smectite to 0.41 and 0.45 nm for the same sequence of anchored clays.

3.3. Infrared spectroscopy

The infrared spectra for natural and chemically modified smectites showed broad bands at 3658 and 3712 cm^{-1}, attributed

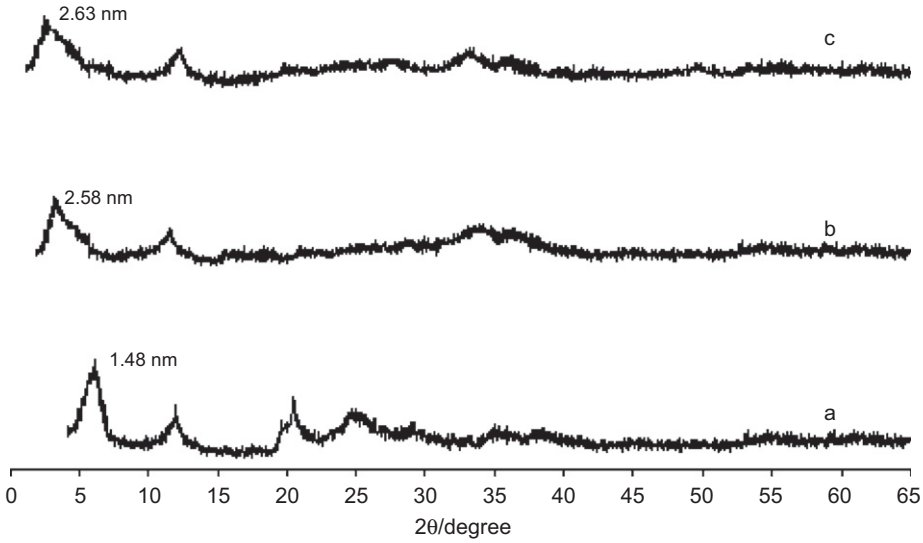

Fig. 1. X-ray diffraction patterns of natural smectite-S (a) and chemical modified smectite samples: $S_{Al/SH}$ (b) and $S_{Zr/SH}$ (c).

Table 1
Basal spacing (d_{001}), surface area (S), micropore area (M), pore volume (P) and pore diameter (PD) for natural and modified smectite samples

Sample	d_{001} (nm)	SA ($m^2 g^{-1}$)	M ($m^2 g^{-1}$)	P ($cm^3 g^{-1}$)	PD (nm)
S	1.48	44	9.2	1.6	0.13
$S_{Al/SH}$	1.78	583	20.1	2.7	0.41
$S_{Zr/SH}$	2.13	585	22.2	3.7	0.45

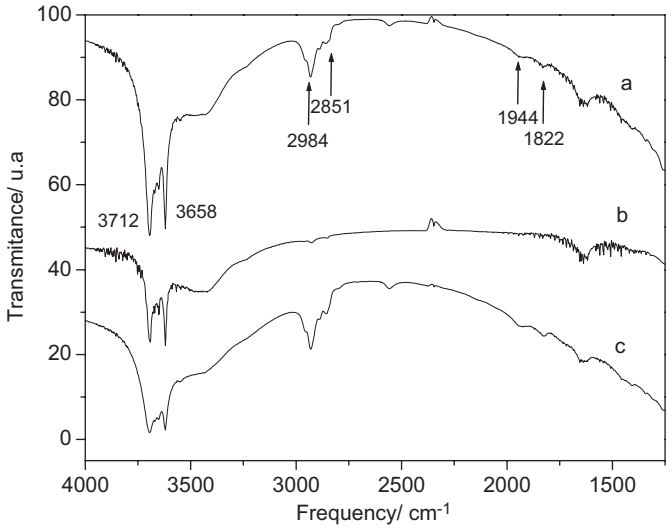

Fig. 2. FTIR spectra of the smectite samples: $S_{Al/SH}$ (a), natural (b) and $S_{Zr/SH}$ (c).

to the OH group, which could be bonded to silicon or aluminum atoms on the inorganic backbone [14]. Such hydroxyl groups can be sited at the corners and fractures of sheets are formed by tetrahedral inversion processes. The new low band at 2984 cm^{-1} probably appeared due to the existence of C–H vibration of the remaining methoxy groups or from CH_2 groups of the chain of the silylating agent, which shows the success of preparing the chemically anchored surface [14]. A weak band at 2851 cm^{-1} was observed in the modified matrix spectra, which was attributed to the O–CH_3 group. Moreover, bands at 1944 and 1822 cm^{-1}, related S–H stretching vibration are observed for the anchored surfaces, corroborating again with the immobilization process, as shown in Fig. 2.

3.4. ^{29}Si NMR

The spectra of the natural and modified montmorillonite samples for silicon are shown in Fig. 3. From the structural point of view, the tetrahedral silicon atom is oxygen bridged to the neighboring silicon, aluminum or zirconium atoms, whose signals at −92.0 and −99.0 ppm are assigned to Q^2 and Q^3, corresponding to $(SiO)_2Si[OSi(M)](OH)$ and $(SiO)_3Si[OSi(M)]$, where the representation Si(M) corresponds to partial substitution on silicon by M (Al or Zr) in the inorganic structure to give the final species [14], as shown in Fig. 3a. For the chemically anchored smectite $S_{Al/SH}$, spectrum peaks at −51.0, −65.0, −91.0 and −99.0 ppm were observed. The first two peaks can be attributed to the presence of organosilane groups R incorporated in the montmorillonite structure as represented by the R–$Si^*[OSi(M)_3]$ form, indicated by T^3, and R–$Si^*[OSi(M)_2](OH)$ that corresponds to T^2. The other two peaks are related to Q^2 and Q^3, respectively, as shown in Fig. 3b. Identically, for $S_{Zr/SH}$ the set of four peaks at 52.0, 66.0, 94.0 and 98.0 ppm were assigned for Q^2, Q^3, T^2 and T^3 peaks, as shown in Fig. 3c. These assignments for T^n species were based on the grafted silylating agent molecule when bonded directly to the inorganic structure. As previously established, the signals resulting from this same anchored molecule on silica gel appeared in the −49.0 to −68.0 ppm range, depending upon the bonding type [14], for alkyltrichlorosilane grafted on layered silicates the signals also appear in the −56.0 to −65.0 ppm interval [15].

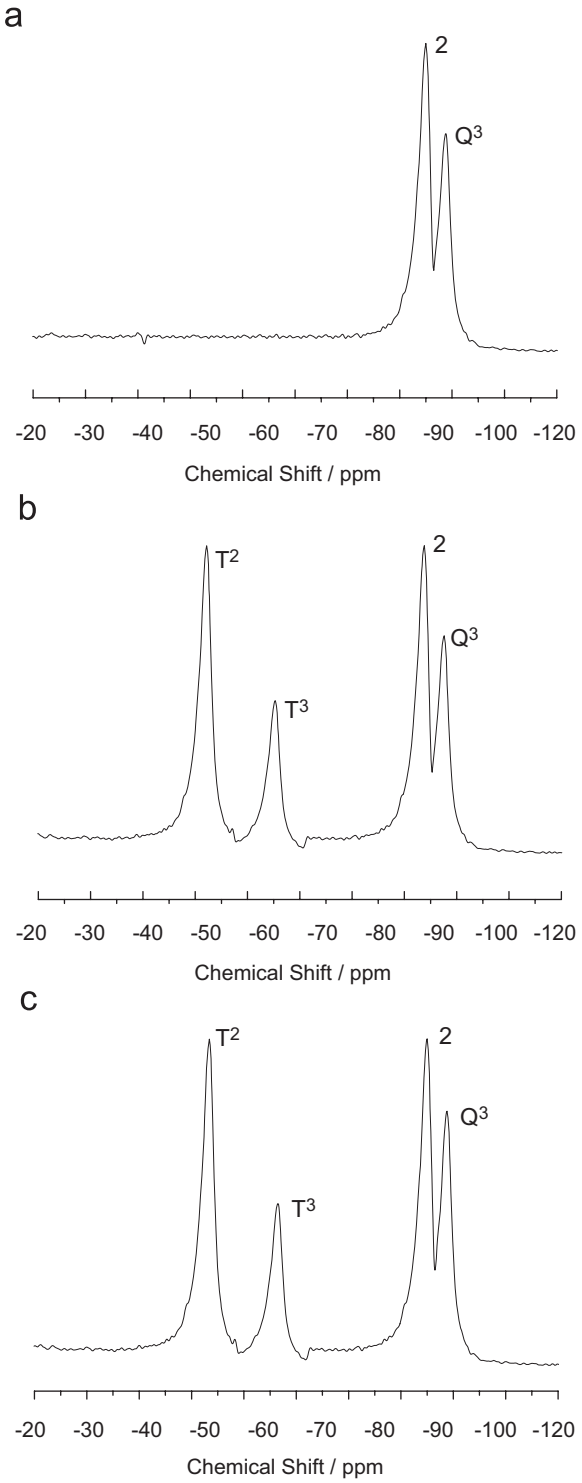

Fig. 3. ^{29}Si-MAS/NMR spectra of modified smectite samples: S (a), $S_{Al/SH}$ (b) and $S_{Zr/SH}$ (c).

3.5. Adsorption study

The divalent adsorptions of metals on natural and chemically immobilized smectites are shown in Figs. 4 and 5. The influence of pillars and the silylating agent on the structure was observed through adsorption values at the saturation of the isotherms. The molecules anchored onto oxides, containing the SH group on pendant chains permit the interaction of this support with cations, due to the presence of the basic reactive center [14,15,18–27]. Based on the structural features presented by the SH groups on the natural or modified pillared clay surfaces, the adsorption can be related directly to the available sulfur atoms. The Langmuir, Redlich–Peterson and Toth nonlinear adsorption models were used to explain the significant capacity of these matrices to quantify divalent metal interactions on these polymeric inorganic structures.

The nonlinear Langmuir model presents a significant advantage when used with these experimental data; it allows quantifying the capacity of cations present to bond to basic centers and to evaluate the constant related to the binding energy [18–26].

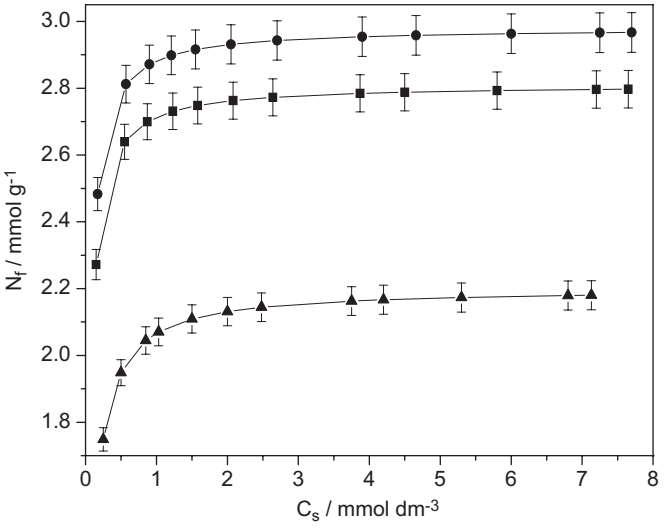

Fig. 4. Adsorption process of copper onto natural S (▲) and modified smectite samples $S_{Al/SH}$ (■) and $S_{Zr/SH}$ (●) (pH 6.0, 360 min and 298 ± 1 K).

The Redlich–Peterson and Toth models were similar to Langmuir model with coefficient r^2 over 0.99 [28,29]. The large capacity of modified smectite samples was confirmed through constant values obtained with these models in the nonlinear form, the results obtained with nonlinear form showed best approximation with experimental data; it is illustrated in Fig. 6 and listed in Table 2. The large capacity of adsorption of the anchored matrix is represented by these constant values and it is attributed to the immobilization of −SH groups on the surfaces. The attached group is the reactive basic center that contributes directly to the adsorption property of the anchored matrices.

The smectite cation adsorption capacity for all these smectite matrices depends on the nature of the complex formed on the surface and also on the affinity of the divalent metal for any particular attached ligand [17,18,21]. The maximum adsorption capacity, N_{fMAX}, for each cation on the organofunctionalized smectite is listed in Table 3, with the highest values for organofunctionalized matrices. When the same anchored matrix is considered, copper is more intensively adsorbed than cobalt. For example, for $S_{Zr/SH}$ matrix the maximum adsorption for cobalt is 3.09 mmol g^{-1} while copper gave 3.50 mmol g^{-1}, showing also an increase of N_{fMAX} with temperature. A possible explanation for this enhancement in adsorption with temperature is the activation of the remaining basic centers of original structure on the clay, possibly arising from displacement of water initially hydrogen bonded to the clay and the pillared surfaces [29]. These N_{fMAX} values reflect the good affinity of the sulfur donor atom attached to the inorganic backbone for bonding copper. A favorable sulfur/copper interaction was previously observed for this same silylating agent immobilized on phyllosilicate [30].

3.6. Thermodynamics of adsorption

The thermodynamic results were obtained from Fig. 7 and the values are listed in Table 3. The Gibbs free energy associated with divalent metal/natural and anchored smectite adsorption can be determined by the Langmuir constant K_L [20–27].

The enthalpy ($\Delta_r h$) is related to the thermal effect per mass for each matrix, $\Delta_{int}h$, which corresponds to the enthalpy of monolayer formation. $\Delta_{int}h$ and K_L values can be determined from coefficients after linearization of the isotherm. The molar enthalpy of the interaction process can be calculated

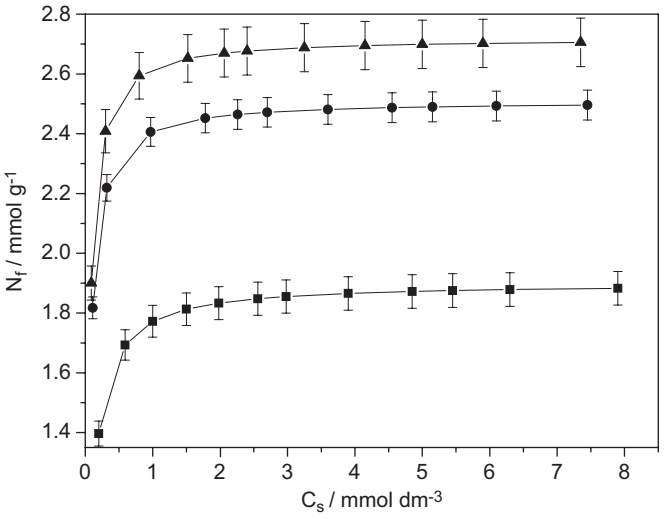

Fig. 5. Adsorption process of cobalt onto natural S (▲) and modified smectite samples $S_{Al/SH}$ (●) and $S_{Zr/SH}$ (■) (pH 6.0, time 360 min and 298 ± 1 K).

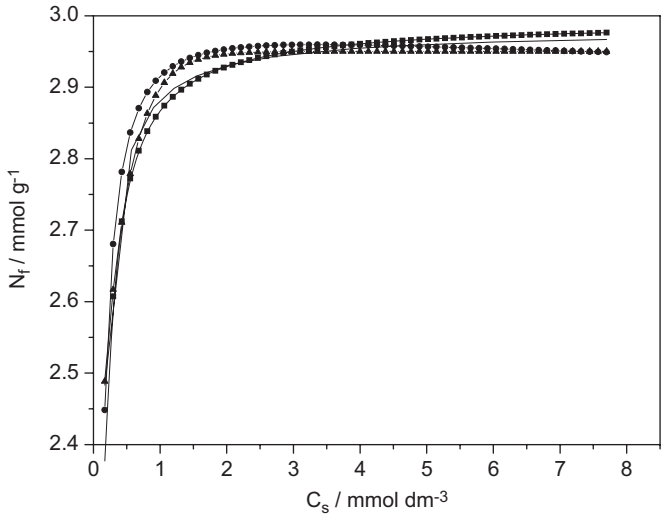

Fig. 6. Experimentally adjusted data with experimental (–) Langmuir (●), Redlich–Peterson (■) and Toth (▲) models.

Table 2
Langmuir, Redlich–Peterson and Toth models applied to divalent metal adsorption on natural and anchored samples, for 3.0 g dm^{-3} of clay with 50.0 mg dm^{-3} initial cation concentrations, pH = 5.0 at 298 ± 1 K

Sample	Langmuir			Redlich–Peterson				Toth			
	b	$K_L \times 10^{-3}$	r^2	N	$K_{RP} \times 10^{-3}$	β	r^2	N	$K_T \times 10^{-3}$	β	r^2
Cu^{2+}											
S	2.2 ± 0.1	15.7 ± 0.1	0.999	2.5 ± 0.1	16.3 ± 0.2	0.5 ± 0.1	0.999	2.6 ± 0.1	16.6 ± 0.1	0.7 ± 0.1	0.998
$S_{Al/SH}$	2.8 ± 0.2	28.2 ± 0.1	0.999	2.9 ± 0.1	29.0 ± 0.1	0.7 ± 0.2	0.989	2.9 ± 0.2	28.8 ± 0.2	0.7 ± 0.2	0.997
$S_{Zr/SH}$	3.0 ± 0.1	29.4 ± 0.1	0.998	3.0 ± 0.1	30.6 ± 0.2	0.9 ± 0.1	0.999	3.0 ± 0.1	31.0 ± 0.1	0.9 ± 0.1	0.999
Co^{2+}											
S	1.9 ± 0.1	13.9 ± 0.1	0.999	2.1 ± 0.1	14.2 ± 0.2	0.5 ± 0.2	0.997	2.2 ± 0.1	13.8 ± 0.1	0.6 ± 0.2	0.997
$S_{Al/SH}$	2.5 ± 0.2	23.8 ± 0.1	0.989	2.5 ± 0.1	24.0 ± 0.1	0.6 ± 0.2	0.998	2.5 ± 0.2	23.9 ± 0.2	0.7 ± 0.1	0.989
$S_{Zr/SH}$	2.7 ± 0.1	25.8 ± 0.2	0.998	2.5 ± 0.2	26.6 ± 0.1	0.8 ± 0.2	0.997	2.6 ± 0.2	25.8 ± 0.2	0.8 ± 0.1	0.989

Table 3
Thermodynamic data for divalent cation adsorption on natural and chemically modified smectite samples, for 3.0 g dm^{-3} of clay, with 50.0 mg dm^{-3} initial cation concentrations, 360 min, pH = 5.0 at 298 ± 1 K

Sample	T (K)	$K_L \times 10^{-3}$	$-\Delta_{hint}$ (J g^{-1})	N_s (mmol g^{-1})	N_{fMAX} (mmol g^{-1})	$-\Delta_{int}G^0$ (kJ mol^{-1})	$-\Delta_{int}H^0$ (kJ mol^{-1})	$\Delta_{int}S^0$ (JK^{-1} mol^{-1})	r^2
Cu^{2+}									
S	303 ± 1	15.7 ± 0.1	13.3 ± 0.1	1.5 ± 0.1	1.9 ± 0.1	23.9 ± 0.1	9.2 ± 0.2	51.3 ± 0.3	
	318 ± 1	16.3 ± 0.1			1.9 ± 0.2	25.6 ± 0.1			0.998
	333 ± 1	16.9 ± 0.1			2.1 ± 0.1	26.9 ± 0.1			
$S_{Al/SH}$	303 ± 1	28.2 ± 0.1	15.8 ± 0.1	1.5 ± 0.1	2.8 ± 0.1	25.8 ± 0.1	10.1 ± 0.1	53.8 ± 0.2	
	318 ± 1	29.5 ± 0.1			2.9 ± 0.2	27.2 ± 0.1			0.997
	333 ± 1	30.8 ± 0.1			2.9 ± 0.2	28.6 ± 0.1			
$S_{Zr/SH}$	303 ± 1	29.4 ± 0.1	19.3 ± 0.1	1.8 ± 0.1	3.0 ± 0.2	25.9 ± 0.1	10.2 ± 0.2	55.0 ± 0.3	
	318 ± 1	30.0 ± 0.1			3.2 ± 0.2	27.3 ± 0.1			0.996
	333 ± 1	31.2 ± 0.1			3.5 ± 0.1	28.7 ± 0.1			
Co^{2+}									
S	303 ± 1	13.9 ± 0.1	13.3 ± 0.1	1.5 ± 0.1	1.9 ± 0.2	24.0 ± 0.1	9.2 ± 0.2	51.2 ± 0.2	
	318 ± 1	14.8 ± 0.1			1.9 ± 0.1	25.4 ± 0.1			0.998
	333 ± 1	17.1 ± 0.1			2.0 ± 0.1	27.0 ± 0.1			
$S_{Al/SH}$	303 ± 1	23.9 ± 0.1	15.4 ± 0.1	1.5 ± 0.1	2.5 ± 0.2	25.4 ± 0.1	9.9 ± 0.3	53.3 ± 0.2	
	318 ± 1	25.6 ± 0.2			2.7 ± 0.1	26.8 ± 0.2			0.997
	333 ± 1	27.5 ± 0.1			2.7 ± 0.1	28.3 ± 0.1			
$S_{Zr/SH}$	303 ± 1	25.8 ± 0.1	19.2 ± 0.2	1.9 ± 0.1	2.7 ± 0.2	25.6 ± 0.1	10.2 ± 0.2	54.9 ± 0.2	
	318 ± 1	28.5 ± 0.1			2.9 ± 0.1	27.1 ± 0.1			0.996
	333 ± 1	30.0 ± 0.2			3.1 ± 0.2	28.5 ± 0.2			

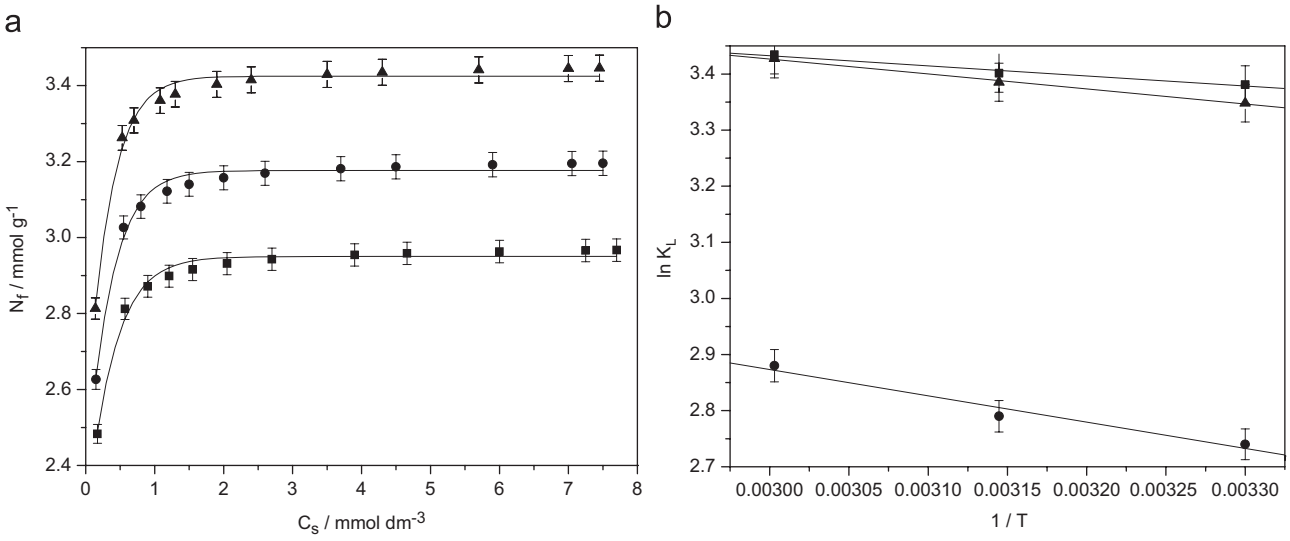

Fig. 7. Experimental thermodynamic data at (a) 303 (■), 318 (●) and 333 K (▲) and (b) van't Hoff linearization.

through [20–27]

$$\Delta_{int}H = \Delta_{int}h/N_S \quad (8)$$

where N_S is the number of adsorbent moles after reaching thermodynamic equilibrium. From K_L values the Gibbs energy is calculated by [18,20–27]:

$$\Delta_{int}G = -RT \ln K_L \quad (9)$$

where T is the absolute temperature and the universal gas constant $R = 8.314 \times 10^{-3}\,kJ\,K^{-1}\,mol^{-1}$, and the entropy values can be calculated by considering [25–33]:

$$\Delta_{int}G = \Delta_{int}H - T\Delta_{int}S \quad (10)$$

The thermodynamic data involving copper and cobalt adsorption are listed in Table 3. The negative Gibbs free energy value for natural smectite is lower than those related to the anchored surfaces and the values increase with temperature, identically for both cations. For the exothermic enthalpic values, those for natural smectite are slightly higher than those obtained with the immobilized smectites. However, the positive entropic data for complexation of these cations also increases from the natural to the anchored smectites. Based on the thermodynamic values obtained, the Gibbs free energy suggests spontaneity of complex formation, corroborating the resulting exothermic enthalpic values as the metal is bonding to the available sulfur in the pendant chains. On the other hand, as the interaction is in progress, the desolvation disturbs the structure of the reaction medium to promote the disorganization of the system and, consequently, leads to an increase in entropy [18,20–27], to yield favorable thermodynamic data for interaction at the solid/liquid interface.

3.7. Kinetic study

When the rate of reaction of an adsorption reaction is controlled by chemical exchange, then a pseudo-second-order model can be best adjusted to the experimental kinetic data, as expressed by [28,29,34–36]

$$\frac{\partial N_t}{\partial t} = k_2(N_{fEQ} - N_f) \quad (11)$$

After integration and applying the boundary conditions, $N_t = 0$ at $t = 0$ and $N_f = N_t$ at $t = t$, the integrated form of Eq. (12) becomes [28]:

$$N_f = \frac{1}{(1/k_2N_{EQ}) + (t/N_{EQ})} \quad (12)$$

where N_{EQ} (mmol g^{-1}) and N_t (mmol g^{-1}) are the amounts of metal adsorbed at equilibrium and at a given time t (min), respectively, and k_2 is the rate constant of pseudo-second-order adsorption (mmol^{-1} min^{-1}).

Carrying out a set of experiments at constant temperature and monitoring the amount adsorbed with time, the kinetics of the adsorption process is calculated. The adsorption kinetics was tested with respect to the well-known Lagergren model and pseudo-second-order kinetics.

The anchored and natural smectite samples showed identical behavior towards cobalt and copper uptake with increasing interaction time at the temperature of these metal solutions. The adsorption increased relativity rapidly up to approximately 120 min and then stabilized as equilibrium was reached, as shown in Figs. 8 and 9. The metal uptake became almost constant after 150 min for natural and after 100 min for anchored smectite samples, which can be considered as reaching equilibrium. The initial high rate of cation adsorption is shown in Figs. 8 and 9, which may be attributed to the existence of the exposed surface. However, as the coverage increased, the number of available surface sites for adsorption decreases until it reaches equilibrium.

Second-order kinetic plots show better nonlinear results with $r^2 > 0.99$ and the second rate constant k_2 varied from 4.8×10^{-2} to 15.0×10^{-2} mmol^{-1} min^{-1} and 3.9×10^{-2} to 12.2×10^{-2} mmol^{-1} min^{-1} for copper and cobalt, respectively, when $S_{Zr/SH}$ matrix is considered, as listed in Table 4. Nonlinear regression provided higher correlation with the experimental data for both kinetic analyses and the present results demonstrated close agreement with reported data [28,29].

The variations of rate constant k_2 are listed in Table 4; this rate increased significantly in the adsorption process with anchored smectite samples and similar behavior is observed for N_f values. The reactive centers inserted by pillarization and organofunctionalization process intervene substantially in the kinetic values. The −SH group is responsible for increasing the number of molecules of copper and cobalt processed per unit time in the complexation with the divalent metal.

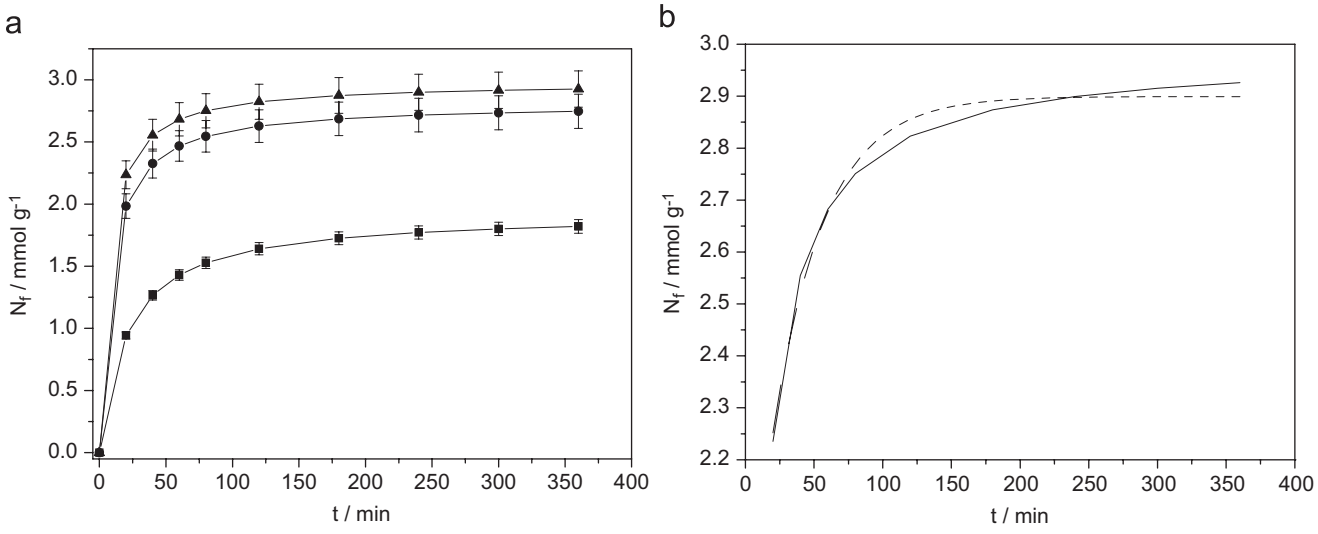

Fig. 8. Experimental kinetic data for adsorption of Cu^{2+} on (a) S (■), $S_{Al/SH}$ (●), $S_{Zr/SH}$ (▲) and (b) adjusted with nonlinear correction.

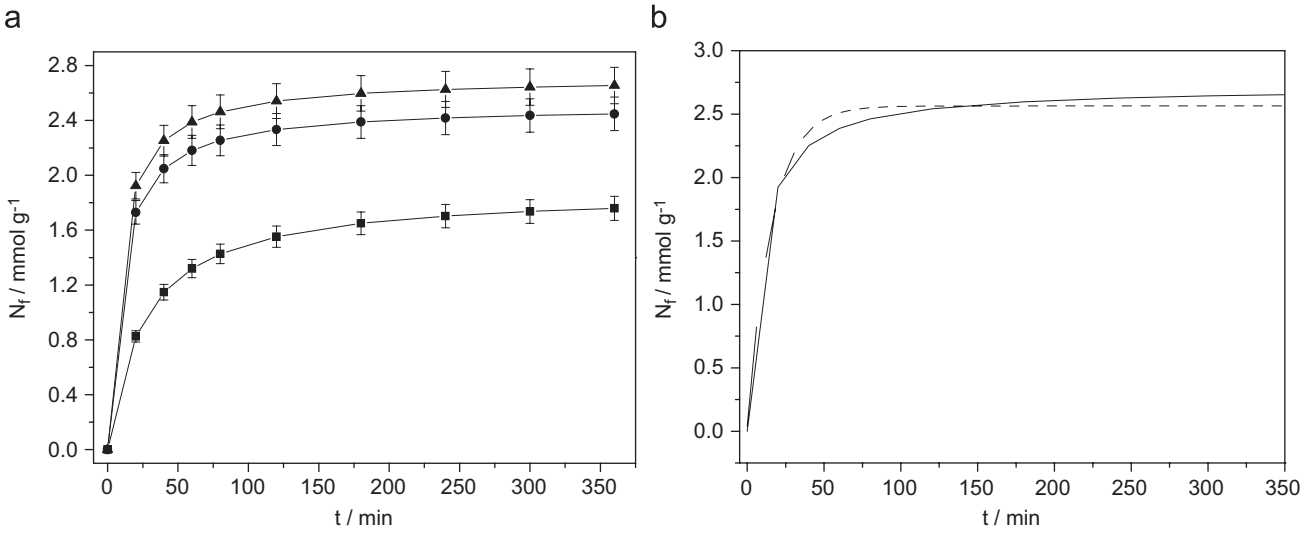

Fig. 9. Experimental kinetic data for adsorption of Co^{2+} on (a) S (■), $S_{Al/SH}$ (●), $S_{Zr/SH}$ (▲) and (b) adjusted with nonlinear correction.

Table 4
Kinetic values calculated for divalent metal adsorption onto natural and modified clay samples, for 3.0 g dm^{-3} of clay, initial cation concentration 50.0 mg dm^{-3}, pH = 5.0, at 298 ± 1 K

Sample	Second-order kinetic equation		
	$k_2 \times 10^{-2}$ (mmol^{-1} min^{-1})	N (mmol g^{-1})	r^2
Cu^{2+}			
S	4.8 ± 0.3	1.9 ± 0.1	0.999
$S_{Al/SH}$	12.0 ± 0.3	2.8 ± 0.2	0.998
$S_{Zr/SH}$	15.0 ± 0.2	3.0 ± 0.2	0.989
Co^{2+}			
S	3.9 ± 0.2	1.9 ± 0.2	0.998
$S_{Al/SH}$	11.1 ± 0.2	2.5 ± 0.2	0.997
$S_{Zr/SH}$	12.2 ± 0.2	2.7 ± 0.2	0.999

4. Conclusion

The chemically modified smectite, originally from the Amazon region, Brazil, has high stability, mainly when reactive sites were introduced, with improvement of physical–chemical properties of the precursor clay mineral. The specific area of the natural smectite, 44 m^2 g^{-1}, increased after the immobilization process to give 585 m^2 g^{-1}. Identically, chemically modified clay samples when applied to the divalent metal adsorption process, increased their capacity for cobalt and copper removal, a favorable condition attributed to the available edge sites on the inorganic backbone, to give the order $Cu^{2+} > Co^{2+}$ with affinities of 3.5 and 3.1 mmol g^{-1}, respectively.

Adsorption on natural or modified smectite clay samples increased continuously with temperature. The most appropriate condition was pH 5.0 at 298 ± 1 K, to present a plateau at 360 min. The uptake of cations was very fast initially for both inorganic supports before reaching the plateau. The Langmuir isotherm yielded good fits with the adsorption data for divalent metal/clay interactions ($r^2 > 0.99$).

The quantitative metal/reactive center interactions of modified smectite clay were followed thought van't Hoff method at the solid/liquid interface to give favorable sets of data, such as exothermic enthalpy, negative Gibbs free energy and positive entropic values. These thermodynamic values suggest the application of this material, available worldwide, to improve the environment as cation extraction agents.

A second-order process can better express the kinetics of both metal adsorptions used in this investigation involving natural and anchored smectites. Nonlinear regression provided high degrees of correlation with experimental data for both kinetic and isothermal analyses.

Acknowledgments

The authors are indebted to CNPq for fellowships and FAPESP for financial support.

References

[1] K.G. Bhattacharyya, S.S. Gupta, Colloids Surf. A 277 (2006) 191.
[2] D.M. Manohar, B.F. Noeline, T.S. Anirudhan, Appl. Clay Sci. 31 (2006) 194.
[3] G. Bayramoglu, S. Bektas, M.Y. Arica, J. Hazard. Mater. 101 (2003) 285.
[4] B. Yu, Y. Zang, A. Shukla, S.S. Shukla, K.L. Dorris, J. Hazard. Mater. 80 (2000) 33.
[5] J.J. Tunney, C. Detellier, Chem. Mater. 8 (1996) 927.
[6] N. Wada, R. Raythatha, S. Minomura, Solid State Commun. 63 (1987) 783.
[7] R.L. Frost, T.H.T. Tran, J. Kristóf, Clay Miner. 32 (1997) 587.
[8] N. Temkin, E. Kadinci, Ö. Demirbas, M. Alkan, A.J. Kara, J. Colloid Interface Sci. 89 (2006) 472.
[9] D.L. Guerra, V.P. Lemos, C. Airoldi, R.S. Angélica, Polyhedron 25 (2006) 2880.
[10] C. Airoldi, S. Roca, J. Mater. Chem. 6 (1996) 1963.
[11] L.M. Nunes, C. Airoldi, J. Solid State Chem. 154 (2000) 557.
[12] L.M. Nunes, C. Airoldi, Mater. Res. Bull. 34 (1999) 2121.
[13] S.C. Tsai, K.W. Juang, J. Radional. Nucl. Chem. 243 (2000) 741.
[14] V.S.O. Ruiz, G.C. Petrucelli, C. Airoldi, J. Mater. Chem. 16 (2006) 2338.
[15] T.R. Macedo, G.C. Petrucelli, C. Airoldi, Clay Clay Miner. 55 (2007) 151.
[16] M. Ogawa, S. Okutomo, K. Kuroda, J. Am. Chem. Soc. 120 (1998) 7361.
[17] K.G. Battacharyya, S.S. Gupta, Separ. Purif. Technol. 50 (2005) 388.
[18] A.G.S. Prado, C. Airoldi, Anal. Chim. Acta 432 (2001) 201.
[19] D.M. Moore, R.C. Reynolds, X-ray Diffraction the Identification Analysis of Clay Minerals, Oxford University Press, 1989, pp. 179–201.
[20] R.S.A. Machado, M.G. Fonseca, L.N.H. Arakaki, S.F. Oliveira, Talanta 63 (2004) 317.
[21] M.O. Machado, A.M. Lazarin, C. Airoldi, J. Chem. Thermodyn. 38 (2006) 130.
[22] V.S.O. Ruiz, C. Airoldi, Thermochim. Acta 420 (2004) 73.
[23] O.A.C. Monteiro, C. Airoldi, J. Colloid Interface Sci. 282 (2005) 32.
[24] A.M. Lazarin, C. Airoldi, J. Mater. Chem. 18 (2006) 2226.
[25] C.B.A. Lima, C. Airoldi, Solid State Sci. 4 (2002) 1321.
[26] M.G. Fonseca, J.A. Simoni, C. Airoldi, Thermochim. Acta 369 (2001) 17.
[27] M.G. Fonseca, C. Airoldi, Thermochim. Acta 359 (2000) 1.
[28] D. Karadag, Y. Koc, M. Turan, M. Ozturk, J. Hazard. Mater. 144 (2007) 432.

[29] Y.S. Ho, Water Res. 40 (2006) 119.
[30] S. Al-Ashem, Z. Duvnjak, Water Air Soil Pollut. 114 (1999) 251.
[31] P.D. Padilha, J.C. Rocha, J.C. Moreira, J.T.D. Campos, C.D. Federici, Talanta 45 (1997) 317.
[32] M.G. Fonseca, C. Airoldi, J. Chem. Soc. Dalton Trans. 42 (1999) 3687.
[33] A.I. Martin, M. Sanchez-Chaves, F. Arranz, React. Funct. Polym. 39 (1999) 179.
[34] Y.S. Ho, G. McKay, Process Biochem. 34 (1994) 431.
[35] M. Martinez, N. Miralles, S. Hidalgo, N. Fiol, I. Villaescusa, J. Poch, J. Hazard. Mater. B 133 (2006) 203.
[36] Y.S. Ho, J. Hazard. Mater. 136 (2006) 681.